Rheol Acta (2017) 56:863–869
DOI 10.1007/s00397-017-1047-7

RAPID COMMUNICATION

Probe microrheology without particle tracking by differential dynamic microscopy

Alexandra V. Bayles[1] · Todd M. Squires[1] · Matthew E. Helgeson[1]

Received: 15 July 2017 / Revised: 30 August 2017 / Accepted: 30 August 2017 / Published online: 19 September 2017

Abstract We present a new method for performing passive probe microrheology. Using a simple theoretical framework, we show how probes' mean-squared displacements can be extracted by analyzing intensity fluctuations in optical microscopy videos via differential dynamic microscopy (DDM). Applying the method to optically dilute probes in Newtonian and viscoelastic fluids quantitatively reproduces mean-squared displacements extracted from multiple particle tracking (MPT), and exposes the relative strengths and weakness of DDM. Furthermore, DDM can be used to measure the mean-squared displcement in optically dense fluids where MPT fails, demonstrating that DDM can extend the range of microrheology experiments while circumventing many of the drawbacks of MPT.

Keywords Microrheology · Viscoelasticity · Differential dynamic microscopy · Mean squared displacement

Introduction

The mechanical properties of soft materials are typically measured with macroscopic rheometers. However, recent decades have seen the development of microrheology, which has enabled deeper characterization of the mechanics and microdynamics of fluids with measurement of smaller sample volumes, weaker moduli, and extended frequency ranges (Furst and Squires 2017). Specifically, passive microrheology characterizes the linear rheological properties of soft materials by measuring the Brownian motion of embedded colloidal probes. Thermally fluctuating probes stress the material, and the material's frequency-dependent mechanical response can be characterized by measuring the probes' collective mean-squared displacement $\langle \Delta r^2 \rangle$ over a lag time Δt.

Multiple particle tracking (MPT) is the conventional tool for acquiring probe microrheology data, in which particles are imaged using video microscopy, and $\langle \Delta r^2(\Delta t) \rangle$ is extracted by identifying particle positions based on their intensity profile and linking them to generate trajectories (Crocker and Grier 1996; Mason et al. 1997; Squires and Mason 2010). While used extensively, MPT is limited to optically dilute materials, and requires probe particles with known intensity profiles. Additionally, MPT requires several user inputs that must be adjusted for each experiment, including intensity profile thresholds and widths, maximum displacements, and the number of frames a probe can skip in a long trajectory before it is declared a different probe. Specific choices for these inputs impact measurement accuracy in a non-obvious way. Even with judiciously chosen inputs, MPT discards a significant fraction of particles that do not meet these criteria that would otherwise contribute to the ensemble. Overcoming these limitations could dramatically expand the range of fluids accessible to passive microrheology, and circumvent the need to tailor fluids toward these measurements.

Here, we show that differential dynamic microscopy (DDM) can be used to extract $\langle \Delta r^2(\Delta t) \rangle$ and linear viscoelastic material functions from passive probe video microscopy.

Electronic supplementary material The online version of this article (https://doi.org/10.1007/s00397-017-1047-7) contains supplementary material, which is available to authorized users.

✉ Matthew E. Helgeson
helgeson@engineering.ucsb.edu

[1] Department of Chemical Engineering, University of California Santa Barbara, 3357 Engineering II, Santa Barbara, CA 93106, USA

DDM does not require these user inputs and therefore overcomes limitations of MPT. We show how the self-intermediate scattering function obtained by DDM can be inverted to obtain $\langle \Delta r^2(\Delta t) \rangle$ over length and time scales comparable to MPT. We then use DDM to perform passive microrheology of Newtonian fluids, viscoelastic wormlike micelles, and cross-linked polymer solutions and gels. These examples include cases where DDM is more robust than MPT and provides better measures of ensemble statistics, and thus reveal DDM to be a powerful, complementary and accessible tool for microrheology.

Theory

Differential dynamic microscopy measures the ensemble dynamics of complex fluids by reconstructing dynamic scattering patterns from video microscopy (Cerbino and Trappe 2008; Giavazzi and Cerbino 2014). The Fourier-based technique has been applied in a range of imaging systems, including bright-field (Ferri et al. 2011; He et al. 2012; Dienerowitz et al. 2013; Gao et al. 2015), fluorescence (He et al. 2012), confocal (Lu et al. 2012), polarized (Giavazzi et al. 2014), phase-contrast (Wilson et al. 2011; Martinez et al. 2012; Reufer et al. 2012) and dark-field (Bayles et al. 2016), making it ideally suited to characterize a broad range of complex fluids. Notable DDM studies have characterized the dynamics of concentrated colloidal dispersions and gels (Ferri et al. 2011; Lu et al. 2012; Gao et al. 2015), active suspensions (Wilson et al. 2011; Lu et al. 2012; Colin et al. 2014; Martinez et al. 2012), and liquid crystals (Giavazzi et al. 2014).

DDM is performed by computing the change in intensity of each pixel $I(\mathbf{x}, t)$ between two micrographs separated by a lag time Δt. The 2D Fourier transform of the difference image $\Delta\hat{I}(\mathbf{q}, \Delta t)$ with the wavevector $\mathbf{q}$ is a convolution of the optical representation of scattering objects and the displacement of their scattering centers over Δt. These two contributions can be decoupled by analyzing the expectation value of the Fourier power spectrum of the difference images (Cerbino and Trappe 2008)

$$D(\mathbf{q}, \Delta t) = \left\langle |\Delta\hat{I}(\mathbf{q}, \Delta t)|^2 \right\rangle. \tag{1}$$

As described previously, $D(\mathbf{q}, \Delta t)$ contains the same autocorrelation function measured in dynamic light scattering (Giavazzi et al. 2009). Traditionally, DDM analysis involves fitting this autocorrelation function to known models of particle motion assumed *a priori* (Wilson et al. 2011; Ferri et al. 2011; Giavazzi et al. 2016). Instead, we show how to extract the 2D $\langle \Delta r^2(\Delta t) \rangle$ from $D(\mathbf{q}, \Delta t)$ without enforcing particular functional forms. Although this approach has been anticipated previously (Giavazzi et al. 2009), to our knowledge it has not yet been demonstrated in experiments.

Consider a series of 2D micrographs of a sample containing N probes in motion. We will assume that the probes are relatively dilute, such that the intensity profile of one probe is insensitive to the locations of other probes. Furthermore, we will assume that the illumination and imaging optics are linear space invariant, i.e., the intensity profile is invariant to linear transforms of the image (Bayles et al. 2016). Under these assumptions, the intensity profile of a probe does not vary at different locations within the imaging plane, and the total micrograph intensity $I(\mathbf{x}, t)$ can be written as

$$I(\mathbf{x}, t) = \sum_{i=1}^{N} I_i(\mathbf{r} - \mathbf{r}_i(t)) + I_B(\mathbf{x}, t), \tag{2}$$

where $\mathbf{r}_i$ is the position of probe i, $I_B(\mathbf{x}, t)$ is the background intensity, and I_i is the generic probe intensity profile. Substituting Eq. 2 into Eq. 1 and simplifying gives

$$\begin{aligned} D(\mathbf{q}, \Delta t) = {} & 2\left|\hat{I}(\mathbf{q})\right|^2 N F(\mathbf{q}, 0) \\ & \times [1 - F(\mathbf{q}, \Delta t)/F(\mathbf{q}, 0)] \\ & + \left\langle \left| \Delta\hat{I}_B(\mathbf{q}, \Delta t) \right|^2 \right\rangle, \end{aligned}$$

where $F(\mathbf{q}, \Delta t)$ is the intermediate scattering function (ISF). The ISF is the spatial Fourier transform of the van Hove correlation function, which quantifies the probability of finding a probe at position $\mathbf{r}$ at $t + \Delta t$ given there is a probe at the origin at t. The ISF can be divided into self and distinct contributions, $F(\mathbf{q}, \Delta t) = F_s(\mathbf{q}, \Delta t) + F_d(\mathbf{q}, \Delta t)$ or

$$F_s(\mathbf{q}, \Delta t) = \left\langle e^{-i\mathbf{q}\cdot(\mathbf{r}_i(t+\Delta t) - \mathbf{r}_i(t))} \right\rangle \tag{3}$$

$$F_d(\mathbf{q}, \Delta t) = \left\langle \sum_{i \neq j}^{N} e^{-i\mathbf{q}\cdot(\mathbf{r}_i(t+\Delta t) - \mathbf{r}_j(t))} \right\rangle. \tag{4}$$

The self-ISF (SISF) reflects the probability that the probe at the origin has moved to $\mathbf{r}$, and the distinct-ISF probability that a different probe has moved to $\mathbf{r}$. We note that $F(\mathbf{q}, 0)$ is the static structure function, $S(\mathbf{q}) = 1 + F_d(\mathbf{q}, 0)$. The distinct ISF vanishes for hydrodynamically dilute, non-interacting scatterers (as is the case for traditional microrheology experiments), so that $S(\mathbf{q}) = 1$ and $F(\mathbf{q}, \Delta t) = F_s(\mathbf{q}, \Delta t)$.

The self-ISF $F_s(\mathbf{q}, \Delta t)$ encodes the distribution of displacements across an ensemble of probes. This distribution has been shown to be exactly Gaussian in special cases, including harmonic solids, ideal gasses, and systems governed by Langevin's equation (Rahman et al. 1962). The distribution of displacements is not necessarily Gaussian in systems where there is spatial and dynamic heterogeneity as in gels (Valentine et al. 2001) and glasses (Weeks et al. 2000).

A more general distribution is captured by expanding $F_s(\mathbf{q}, \Delta t)$ as Nijboer and Rahman (1966)

$$F_s(\mathbf{q}, \Delta t) = e^{\frac{-q^2\left\langle \Delta r^2(\Delta t)\right\rangle}{4}}\left[1 + \frac{\alpha_2 q^4 \left\langle \Delta r^2(\Delta t)\right\rangle^2}{32} + \ldots\right], \tag{5}$$

where the first order non-Gaussian parameter $\alpha_2 = \left(d\left\langle \Delta r^4(\Delta t)\right\rangle\right) / \left((d+2)\left\langle \Delta r^2(\Delta t)\right\rangle^2\right) - 1$ (d is the dimensionality) measures heterogeneity (Weeks et al. 2000).

In principle, a closure approximation is required to compute the higher order terms in Eq. 5 to solve for $\left\langle \Delta r^2(\Delta t)\right\rangle$ and higher-order moments of the displacement distribution, including α_2. However, with a sufficiently large sample of displacements in a homogeneous ensemble, the distribution of thermally driven displacements is expected to be Gaussian, and higher order moments of Eq. 5 can be neglected, i.e. $\alpha_2 = 0$. Substituting Eq. 5 into the dilute, non-interacting version of Eq. 3 allows us to solve for $\left\langle \Delta r^2(\Delta t)\right\rangle$ directly

$$\left\langle \Delta r^2(\Delta t)\right\rangle = \frac{4}{q^2}\ln\left[\frac{A(q)}{A(q) - D(q, \Delta t) + B(q)}\right], \tag{6}$$

where $A(q) = 2\left|\hat{I}(\mathbf{q})\right|^2 N$ and $B(q) = \left\langle\left|\Delta\hat{I}_B(\mathbf{q}, \Delta t)\right|^2\right\rangle$. Direct measures of $A(q)$, the Fourier transformed probe intensity profile, and $B(q)$, the incoherent background, are not required to measure $\left\langle \Delta r^2(\Delta t)\right\rangle$; they can be fit from the $D(q, \Delta t)$ signal.

We now outline how to obtain $\left\langle \Delta r^2(\Delta t)\right\rangle$ from measured $D(q, \Delta t)$ using Eq. 6. Figure 1 depicts $D(q, \Delta t)$ measured for dilute Au nanoparticles (AuNPs) dispersed in a Newtonian sucrose solution. From Eq. 3, it is evident that as $\Delta t \to 0$, $D(q, \Delta t) \to B(q)$. We find that $B(q)$ is well approximated by $min[D(q, \Delta t_{min})]$ provided that the frame rate is sufficiently small and that the background noise is uncorrelated. Though this approximation overestimates $B(q)$, the uncertainty in $A(q)$ dominates uncertainty in the MSD. As $\Delta t \to \infty$, $D(q, \Delta t \to \infty) \to A(q) + B(q)$; thus, $A(q)$ can be extracted from the long Δt plateau. To ensure that $D(q, \Delta t)$ values at high q and long Δt are not used to calculate large displacements, we truncate the calculation of $\left\langle \Delta r^2(\Delta t)\right\rangle$ at Δt where $D(q, \Delta t)$ exceeds 80% of $A(q) + B(q)$. Additionally, we exclude curves for which $D(q, \Delta t)$ does not approach and sustain an appreciable plateau. Excluded data typically correspond to low-q regions (large displacements) where the video is too short to adequately sample $D(q, \Delta t)$, or high-q regions where video frame rate and out-of-plane intensity fluctuations introduce errors. Criteria for excluding q on the basis of standard deviation in the plateau is given in the SI. The statistical tolerance for accepting $A(q)$ is the only user input in DDM analysis.

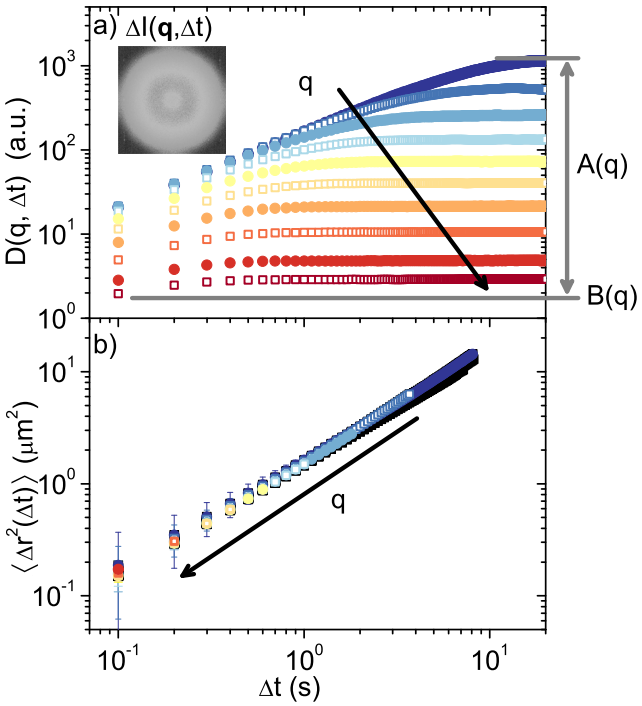

Fig. 1 Measuring $\left\langle \Delta r^2(\Delta t)\right\rangle$ using DDM. **a** Radial average of $D(\mathbf{q}, \Delta t)$ of AuNPs in 50wt% sucrose solution. $B(q)$ and $A(q)+B(q)$ are obtained from short and long Δt limits of $D(q, \Delta t)$. **b** $\left\langle \Delta r^2(\Delta t)\right\rangle$ is calculated using Eq. 6. Colors illustrate short Δt truncation of $\left\langle \Delta r^2(\Delta t)\right\rangle$ at high q. Error bars demark propagated error from $A(q)$ calculation; the majority of error bars are smaller than the markers

Results and discussion

Having established this basic framework, we now demonstrate its utility for microrheology using three canonical soft material systems: AuNPs dispersed in Newtonian sucrose solutions, polystyrene particles dispersed in wormlike micelle solutions, and polystyrene particles dispersed in polyacrylamide gels. In each example, we calculate $D(q, \Delta t)$ using the Matlab software package *DDMCalc* described in Bayles et al. (2016).

Newtonian Au nanoparticle dispersions

To demonstrate the accuracy of DDM in measuring $\left\langle \Delta r^2(\Delta t)\right\rangle$, we prepared dispersions of AuNPs of diameter $2a = 100$ nm in 30, 40 and 50 wt% aqueous sucrose solutions, and recorded their Brownian motion using dark-field microscopy (see Bayles et al. (2016) for experimental details). At low concentrations (volume fraction $\phi = 5 \times 10^{-8}$), the dispersions are dilute in both hydrodynamical

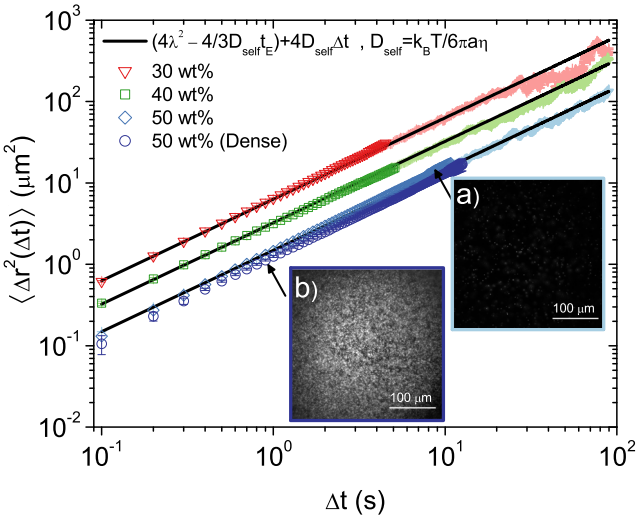

Fig. 2 AuNP $\langle \Delta r^2(\Delta t) \rangle$ measured using DDM (open symbols) agree well with those measured using MPT (filled symbols) in optically dilute AuNP dispersions (micrograph pictured in inset **a**). In optically dense dispersions (inset b), DDM can be used to measure $\langle \Delta r^2(\Delta t) \rangle$ where MPT fails. Solid line indicates fit (which accounts for static and dynamic tracking error) used to obtain AuNP self-diffusivity D_{self}. Error bars indicate the standard deviation of $\langle \Delta r^2(\Delta t) \rangle$ calculated for each Δt across accepted q values

and optical senses: particle intensity profiles are isolated enough for traditional MPT to be performed (see micrograph in Fig. 2a). In MPT, static and dynamic particle tracking errors are accounted for during $\langle \Delta r^2(\Delta t) \rangle$ fitting, as suggested in Fig. 2 and described in detail in Bayles et al. (2016). In DDM, the contribution of static error (incoherent image intensity fluctuations) to the MSD is accounted for by $B(q)$. Dynamic error is manifest in the probe intensity profile encoded in $A(q)$, although its exact contribution to the MSD requires further analysis. Nevertheless, mean-squared displacements extracted from videos using both DDM and MPT algorithms show excellent agreement.

In contrast, MPT is generally impossible in optically dense suspensions, whereas DDM retains accuracy. This is evident in a suspension of 100 nm AuNPs dispersed in 50 wt% aqueous sucrose solutions at $\phi = 3 \times 10^{-5}$. At this volume fraction, probes are hydrodynamically dilute, yet their particle intensity profiles overlap significantly across the image (Fig. 2b). While MPT fails in these suspensions, DDM continues to successfully extract $\langle \Delta r^2(\Delta t) \rangle$. As expected for a purely viscous solution, measured $\langle \Delta r^2(\Delta t) \rangle$ scales linearly with Δt, and the sucrose solution viscosity can be accurately measured via the probe self-diffusivity.

We note that in optically dilute experiments, MPT can be used to measure $\langle \Delta r^2(\Delta t) \rangle$ for lag times up to the entire length of the video. However, these values are typically averaged from such small ensembles (< 1000 displacements) that they are statistically dubious, as evidenced by the scatter of the values. These displacements are usually excluded when fitting $\langle \Delta r^2(\Delta t) \rangle$ to measure fluid properties. In the model-free method of DDM analysis presented here, including only q values that decorrelate over the course of the experiment effectively excludes large displacements that are statistically indeterminate. In principle, this statistical limit could be circumvented and $\langle \Delta r^2(\Delta t) \rangle$ measured by assuming a functional form for the ISF, and fitting $D(q, \Delta t)$. This, however, would require *a priori* knowledge of the viscoeastic properties of the material being characterized, which highlights the need for a model-free approach as illustrated in the following example.

Viscoelastic wormlike micelles

A wormlike micelle solution (12.5 mM sodium salicylate (NaSal) and 15 mM cetylpyridinium chloride (CPyCl)) forms an entangled network with an average mesh size of ~ 300 nm based on the plateau modulus (Rehage and Hoffmann 1991). Polystyrene probes of diameter $2a = 860$ nm were dispersed in the solution at an optically dilute $\phi = 3 \times 10^{-4}$, the solution was sealed in capillary tubes, and probe motion was imaged using fluorescent microscopy on a temperature-controlled stage. A CCD Andor CLARA camera was used to acquire 512x512 pixel videos at 10 Hz with an exposure time of 40 ms.

Figure 3a shows the mean-squared displacement of probe particles in the WLM solution. As with the viscous sucrose solutions, DDM and MPT show excellent agreement in their measured $\langle \Delta r^2(\Delta t) \rangle$. DDM measurements show less noise in $\langle \Delta r^2(\Delta t) \rangle$ for long Δt. Because DDM retains all dynamic information encoded in the video images, statistics are improved. Unlike MPT, no probe displacements are rejected in DDM, causing more displacements to contribute to the ensemble, and ultimately yielding higher precision.

In various forms of microrheology, viscoelastic moduli can be determined from the SISF (Dasgupta et al. 2002; Papagiannopoulos et al. 2005) or from the probe $\langle \Delta r^2(\Delta t) \rangle$. The Generalized Stokes-Einstein relation relates the complex shear modulus $G^*(\omega)$ to $\langle \Delta r^2(\Delta t) \rangle$

$$G^*(\omega) = \frac{2k_B T}{3\pi a i \omega \mathcal{F}\left[\langle \Delta r^2(\Delta t) \rangle\right]}. \tag{7}$$

The mean-square displacement exhibits a power law dependence on lag time, $\langle \Delta r^2(\Delta t) \rangle \sim \Delta t^{\alpha}$, where the Δt dependence of the logaritmic slope α reflects the frequency dependent moduli of the fluid. At short Δt, $\alpha < 0.5$, reflecting the elastic response of the micelles at high ω. At long Δt, α approaches unity, reflecting the viscous domination at low ω. Figure 3b shows the agreement between moduli measured by MPT, DDM and bulk rheology measurements on an ARG2 stress-controlled rheometer with a cone and plate geometry. Some discrepancy in G'' is evident between the

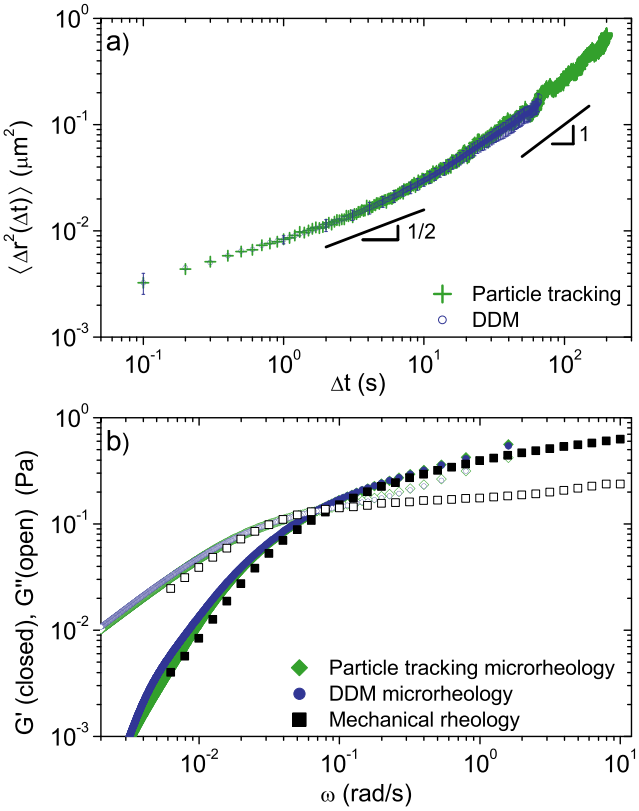

Fig. 3 **a** Mean-squared displacement of polystyrene probes in a viscoelastic WLM solution at 25 °C measured using DDM and MPT. Error bars indicate the standard deviation of $\langle \Delta r^2(\Delta t) \rangle$ calculated for each Δt across accepted q values. **b** Storage (closed symbols) and loss (open symbols) moduli measured extracted from $\langle \Delta r^2(\Delta t) \rangle$ agree well with those measured using macroscopic oscillatory rheometry

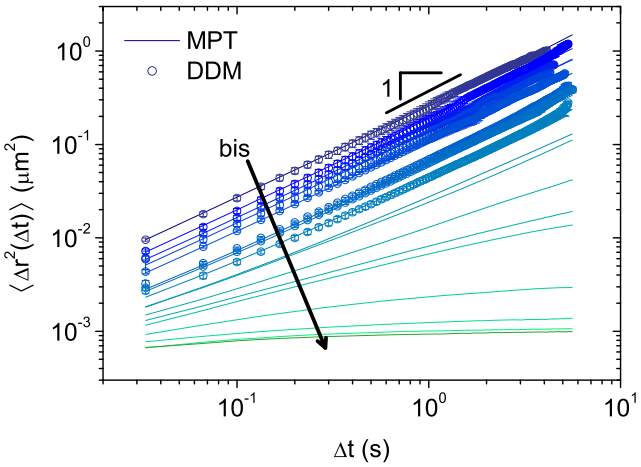

Fig. 4 $\langle \Delta r^2(\Delta t) \rangle$ of polystyrene probes dispersed in polyacrylamide gels with bis-acrylamide crosslinker ranging in concentration from 0.00 wt% (dark blue) to 0.08 wt% (green). $\langle \Delta r^2(\Delta t) \rangle$ measured using DDM agree well with those measured via MPT for sufficiently large displacements where the concentration of bis-acrylamide is < 0.055 wt%. Error bars indicate the standard deviation of $\langle \Delta r^2(\Delta t) \rangle$ calculated for each Δt across accepted q values

microrheology methods (both MPT and DDM) at $\omega > 0.2$ rad/s, possibly due to non-continuum effects related to the similarity of the probe and micelle mesh size.

Crosslinked polyacrylamide solutions and gels

Finally, we use both MPT and DDM to determine $\langle \Delta r^2(\Delta t) \rangle$ for polystyrene probes of diameter $2a = 1.05$ µm dispersed in crosslinked polyacrylamide solutions and gels from fluorescent video microscopy obtained by Larsen and Furst (2008). The extent of crosslinking in these materials is controlled by the amount of bis-acrylamide. The material transitions from a purely viscous polymer solution to a percolated, elastic gel as the bis-acrylamide concentration increases from 0.0 to 0.08 wt%, corresponding with a decrease in α. The rheological properties of the gels, as well as the sol-gel transition can be quantitatively mapped via $\langle \Delta r^2(\Delta t) \rangle$.

We focus on the differences in measuring $\langle \Delta r^2(\Delta t) \rangle$ using DDM and MPT. At low bis-acrylamide concentrations where probe displacements are large, $\langle \Delta r^2(\Delta t) \rangle$ is successfully extracted from DDM, and the results agree well with MPT (Fig. 4). At higher concentrations, however, the probes move, on average, less than the decay length of $I_i(r)$ during the 30 s video. Consequently, $D(q, \Delta t)$ does not decorrelate for length scales smaller than the decay of $\hat{I}(\mathbf{q})$. In such cases, $A(q)$ cannot be accurately fit, and $\langle \Delta r^2(\Delta t) \rangle$ cannot be measured via DDM using a model-free approach. Although $\langle \Delta r^2(\Delta t) \rangle$ could be extracted in principle using the highest q values, we find that $D(q, \Delta t)$ does not sustain a plateau at these high q values (see SI Fig. S5), limiting their utility. We speculate that at high q values, out-of-plane intensity fluctuations are on the same order of magnitude as the in-plane intensity fluctuations, limiting measurement of $\langle \Delta r^2(\Delta t) \rangle$. Excursions of probes outside the boundaries of the image also limit analysis of the highest q values as described by Giavazzi et al. (2017).

As illustrated by this example, the lowest measurable $\langle \Delta r^2(\Delta t) \rangle$ is set by the maximum q value for which $A(q)$ and $B(q)$ can be adequately resolved. The theoretical upper limit of this q value is set by the absolute size of the imaging system. Provided the total particle displacement is greater than the pixel size, $D(q, \Delta t)$ should decorrelate, and subpixel displacements can be measured at small Δt. Practically, out-of-plane probe motion and excursions of outside the image boundaries limit resolvable q values further, and subsequently reduce $\langle \Delta r^2(\Delta t) \rangle$ resolution.

Conclusions

To summarize, we have shown how to invert the SISF obtained by DDM to obtain the real-space $\langle \Delta r^2(\Delta t) \rangle$ without

imposing particular functional forms, thus enabling the use of DDM for passive microrheology measurements. As demonstrative examples, we applied DDM to videos of dilute probes in Newtonian fluids, viscoelastic wormlike micelles, and crosslinking polymer gels. For sufficiently large displacements, the $\langle \Delta r^2(\Delta t) \rangle$ obtained by DDM is nearly indistinguishable from that obtained by MPT. Successful extraction of $\langle \Delta r^2(\Delta t) \rangle$ from optically dense dispersions of AuNPs in sucrose solutions demonstrate the robustness of DDM compared to MPT. WLM experiments demonstrate that DDM microrheological data compares well with mechanical rheological data vis-à-vis the Generalized Stokes-Einstein Relation, and additionally illustrates the improved ensemble sampling of DDM compared to MPT. Conversely, in the limit of small displacements, the sub-pixel tracking algorithms of MPT provide more accurate measurements of $\langle \Delta r^2(\Delta t) \rangle$ than DDM. Although these examples help to identify the relative strengths of DDM and MPT in various limits, a more systematic analysis of these limits, how they can be overcome, and the effect of static and dynamic error requires further study. Nevertheless, our results show that DDM can extend the range of probe microrheology experiments to fluids inaccessible to MPT, while circumventing many of the drawbacks of MPT.

Acknowledgements We thank E. Furst for discussion and collaboration, L. Josephson and T. Larsen for providing polyacrylamide microscopy videos. Funding for this work was provide by the National Science Foundation (DGE1144085, CBET 1438779, and CBET 1351371).

During press of this publication, Edera et al. (2017) posted a manuscript under review that also uses DDM to extract the MSD and thus perform microrheology. Our two approaches share much in common, differing in the materials that are studied, and the generality with which different aspects and features are discussed and derived. Of particular note is their optimization-based method to determine $A(q)$ and $B(q)$, which may extend the useful range of DDM microrheology.

References

Bayles AV, Squires T, Helgeson ME (2016) Dark-field differential dynamic microscopy. Soft Matter 12:2440–2452. https://doi.org/10.1039/C5SM02576A, http://pubs.rsc.org/en/Content/ArticleLanding/2016/SM/C5SM02576A

Cerbino R, Trappe V (2008) Differential dynamic microscopy: Probing wave vector dependent dynamics with a microscope. Phys Rev Lett 100(18):188,102. https://doi.org/10.1103/PhysRevLett.100.188102

Colin R, Zhang R, Wilson L (2014) Fast, high-throughput measurement of collective behaviour in a bacterial population. J R Soc Interface 11(98):1742–5662. http://rsif.royalsocietypublishing.org/content/11/98/20140486.short

Crocker J, Grier D (1996) Methods of digital video microscopy for colloidal studies. J Colloid Interface Sci 310(179):298–310

Dasgupta BR, Tee SY, Crocker JC, Frisken BJ, Weitz DA (2002) Microrheology of polyethylene oxide using diffusing wave spectroscopy and single scattering. Phys Rev E 65(5 Pt 1):51,505. https://doi.org/10.1103/PhysRevE.65.051505, http://www.ncbi.nlm.nih.gov/entrez/query.fcgi?cmd=Retrieve&db=PubMed&dopt=Citation&list_uids=12059562

Dienerowitz M, Lee M, Gibson G, Padgett M (2013) Measuring nanoparticle flow with the image structure function. Lab on a Chip 13(12):2359–23563. https://doi.org/10.1039/c3lc00028a, http://www.ncbi.nlm.nih.gov/pubmed/23644980

Edera P, Bergamini D, Trappe V, Giavazzi F, Cerbino R (2017) Differential Dynamic Microscopy microrheology of soft materials: a tracking-free determination of the frequency-dependent loss and storage moduli. arXiv:1708.07170

Ferri F, D'Angelo a, Lee M, Lotti a, Pigazzini MC, Singh K, Cerbino R (2011) Kinetics of colloidal fractal aggregation by differential dynamic microscopy. European Phys J Special Topics 199(1):139–148. https://doi.org/10.1140/epjst/e2011-01509-9

Furst EM, Squires TM (2017) Microrheology, 1st edn. Clarendon Press, Oxford

Gao Y, Kim J, Helgeson ME (2015) Microdynamics and arrest of coarsening during spinodal decomposition in thermoreversible colloidal gels. Soft Matter 11:6360–6370. https://doi.org/10.1039/C5SM00851D, http://pubs.rsc.org/en/Content/ArticleLanding/2015/SM/C5SM00851D

Giavazzi F, Cerbino R (2014) Digital Fourier microscopy for soft matter dynamics. J Opt 16:083,001. https://doi.org/10.1088/2040-8978/16/8/083001, http://stacks.iop.org/2040-8986/16/i=8/a=083001?key=crossref.0d83eaecaf7975a904e590d19a50d64a

Giavazzi F, Brogioli D, Trappe V, Bellini T, Cerbino R (2009) Scattering information obtained by optical microscopy: differential dynamic microscopy and beyond. Phys Rev E 80(3):031,403. https://doi.org/10.1103/PhysRevE.80.031403

Giavazzi F, Crotti S, Speciale A, Serra F, Zanchetta G, Trappe V, Buscaglia M, Bellini T, Cerbino R (2014) Viscoelasticity of nematic liquid crystals at a glance. Soft Matter 10(22):3938–3949. https://doi.org/10.1039/c4sm00145a, http://www.ncbi.nlm.nih.gov/pubmed/24728549

Giavazzi F, Savorana G, Vailati A, Cerbino R (2016) Structure and dynamics of concentration fluctuations in a non-equilibrium dense colloidal suspension. Soft Matter 12:19–21. https://doi.org/10.1039/C6SM00935B, http://pubs.rsc.org/en/Content/ArticleLanding/2016/SM/C6SM00935B

Giavazzi F, Edera P, Lu PJ, Cerbino R (2017) Correcting artifacts from finite image size in differential dynamic microscopy. arXiv:170707501 pp 1–8

He K, Spannuth M, Conrad J, Krishnamoorti R (2012) Diffusive dynamics of nanoparticles in aqueous dispersions. Soft Matter 8:11,933–11,938. https://doi.org/10.1039/c2sm26392k, http://pubs.rsc.org/en/content/articlehtml/2012/sm/c2sm26392k

Larsen TH, Furst EM (2008) Microrheology of the liquid-solid transition during gelation. Phys Rev Lett 100(14):1–4. https://doi.org/10.1103/PhysRevLett.100.146001

Lu PJ, Giavazzi F, Angelini TE, Zaccarelli E, Jargstorff F, Schofield AB, Wilking JN, Romanowsky MB, Weitz DA, Cerbino R (2012) Characterizing concentrated, multiply scattering, and actively driven fluorescent systems with confocal differential dynamic microscopy. Phys Rev Lett 108(21):218,103. https://doi.org/10.1103/PhysRevLett.108.218103

Martinez VA, Besseling R, Croze OA, Tailleur J, Reufer M, Schwarz-Linek J, Wilson LG, Bees M, Poon WCK (2012) Differential dynamic microscopy: a high-throughput method for characterizing the motility of microorganisms. Biophysical J 103

(8):1637–1647. https://doi.org/10.1016/j.bpj.2012.08.045, http://www.pubmedcentral.nih.gov/articlerender.fcgi?artid=3475350&tool=pmcentrez&rendertype=abstract

Mason TG, Ganesan K, van Zanten J, Wirtz D, Kuo S (1997) Particle tracking microrheology of complex fluids. Phys Rev Lett 79(17):3282–3285. https://doi.org/10.1103/PhysRevLett.79.3282

Nijboer B, Rahman A (1966) Time expansion of correlation functions and the theory of slow neutron scattering. Physica 32(2):415–432. https://doi.org/10.1016/0031-8914(66)90068-1, http://linkinghub.elsevier.com/retrieve/pii/0031891466900681

Papagiannopoulos A, Waigh T, Fluerasu A, Fernyhough C, Madsen A (2005) Microrheology of polymeric solutions using x-ray photon correlation spectroscopy. J Phys: Condensed Matter 17(25):L279–L285. https://doi.org/10.1088/0953-8984/17/25/L06, http://stacks.iop.org/0953-8984/17/i=25/a=L06?key=crossref.fb0fd718bf6820f12deb5e805c710379

Rahman A, Singwi KS, Sjolander A (1962) Theory of slow neutron scattering by liquids. I Phys Rev 126(3):986–996

Rehage H, Hoffmann H (1991) Viscoelastic surfactant solutions: model systems for rheological research. Mol Phys 74(5):933–973. https://doi.org/10.1080/00268979100102721

Reufer M, Martinez VA, Schurtenberger P, Poon WCK (2012) Differential dynamic microscopy for anisotropic colloidal dynamics. Langmuir 28(10):4618–4624. https://doi.org/10.1021/la204904a, http://www.ncbi.nlm.nih.gov/pubmed/22324390

Squires TM, Mason TG (2010) Fluid mechanics of microrheology. Ann Rev Fluid Mech 42(1):413–438. https://doi.org/10.1146/annurev-fluid-121108-145608

Valentine MT, Kaplan PD, Thota D, Crocker JC, Gisler T, Prud'homme RK, Beck M, Weitz DA (2001) Investigating the microenvironments of inhomogeneous soft materials with multiple particle tracking. Phys Rev E 64(6):061,506. https://doi.org/10.1103/PhysRevE.64.061506

Weeks ER, Crocker JC, Levitt AC, Schofield AB, Da Weitz (2000) Three-dimensional direct imaging of structural relaxation near the colloidal glass transition. Science 287(5453):627–631. https://doi.org/10.1126/science.287.5453.627

Wilson LG, Martinez VA, Schwarz-Linek J, Tailleur J, Bryant G, Pusey PN, Poon WCK (2011) Differential dynamic microscopy of bacterial motility. Phys Rev Lett 106(1):018,101. https://doi.org/10.1103/PhysRevLett.106.018101